Three Dimensionally Diluted Magnetic Semiconductor Clusters $Cd_{1-y}Mn_yS$ with a Range of Sizes and Compositions: Dependence of Spectroscopic Properties on the Synthesis Mode

L. Levy,[†,‡] N. Feltin,[†,‡] D. Ingert,[†,‡] and M. P. Pileni*[,†,‡]

Laboratoire SRSI, URA CNRS 1662, Universite P et M Curie, (Paris VI), BP 52, 4 Place Jussieu, 75231 Paris Cedex 05, France, and CEA-CE Saclay, DRECAM-SCM, 91191 Gif sur Yvette, Cedex, France

Received: March 18, 1997; In Final Form: July 24, 1997[⊗]

Absorption and photoluminescence spectroscopic measurements are presented for particles with sizes from 2 to 4 nm, composition from $y = 0$ to 0.3,where y is given by $Cd_{1-y}Mn_yS$, and different preparation modes. No monotonous variation of bandgap energy with increasing composition is observed. The depth of the minimum increases with decreasing particle size. This is attributed to a marked increase in the interactions between the Mn^{2+} d electrons and the valence and conduction band electrons. Mn^{2+} photoluminescence is observed at 77 K, when the particles are aged in the solution. Otherwise only the trap emissions due to CdS defect states are seen. Certain preparation modes favor Mn^{2+} photoluminescence at room temperature.

I. Introduction

The fabrication of assemblies of perfect nanometer-scale crystallites (quantum crystal), identically replicated in unlimited quantities in such a state that they can be manipulated and understood as pure macromolecular substances, is an ultimate challenge of modern materials research with outstanding fundamental and potential technological consequences. These potentialities are mainly due to the unusual dependence of the electronic properties on the particle size, either for metal[1−4] or semiconductor[1,5−18] or diluted magnetic semiconductor[19−26] particles, in the 1−10 nm range.

Type II−VI diluted magnetic semiconductors (DMSs)[27] are semiconductors where host cations (II) are randomly substituted by magnetic ions, Mn^{2+}. The presence of localized magnetic ions in a semiconductor alloy leads to exchange interactions between s−p band electrons and the Mn^{2+}d electrons. This sp−d exchange interaction constitutes a unique interplay between optical properties and magnetism. It plays a double role in determining optical properties: (i) The bandgap of the compound is altered depending upon the concentration of manganese ions. (ii) The 3d levels of transition metal ions are located in the bandgap region, and d−d transitions dominate the spectrum.

DMS bulk-phase bandgaps have been measured at various manganese ions concentrations. A typical nonlinear variation of the bandgap with composition was observed.[28] The deviation from linearity may lead to the presence of a bandgap minimum. Traces of Mn^{2+} included in II−VI semiconductors result in a number of isolated tetrahedrally coordinated Mn^{2+} ions which induce luminescence. This is attributed to energy transfer from host semiconductor to Mn^{2+} ions.[22,27,29] Thus, the absorption, photoconductivity, and photoluminescence spectra are highly structured and provide basic information for understanding optical processes in DMS materials.[30] The DMS shows a variety of marked magnetooptical properties due to the exchange interaction of the band electrons with the magnetic ions.[31] The sp−d spin exchange interaction constitutes a unique magnetism interplay and results in unusual magnetotransport and magnetooptic phenomena such as a large Faraday rotation, giant negative magnetoresistance, and magnetic field induced metal−insulator transitions.[29]

In the nanometer-size crystallites of semimagnetic semiconductors, many of these properties are expected to be influenced by the quantum confinement of the electronic states and to be different from those of the bulk crystals. Due to the quantum dot's unique properties, these nanostructures have a great potential for a variety of applications. Recent work on manganese-doped nanocrystals suggests that doped nanocrystals are a new class of materials.[21]

In a previous paper,[32] we demonstrated that the size and composition of $Cd_{1-y}Mn_yS$ nanocrystals can be independently controlled. This is possible by using reverse micelles as microreactors. The particles are extracted from micelles and dispersed in an apolar solvent. Control of the average size (from 1.8 to 4.2 nm) and composition (from $y = 0.03$ to 0.3) is obtained. It was shown by EPR spectroscopy that Mn^{2+} ions are included and randomly dispersed inside the CdS matrix.

We give here the spectroscopic data obtained for particles with different preparation modes.

II. Experimental Section

Products. Sodium bis(ethyl-2-hexyl)sulfosuccinate, Na(AOT), was from Sigma and sodium sulfide (Na_2S) from Janssen. The solvents isooctane, isopentane, and methylcyclohexane were obtained from Fluka, ethanol was from Prolabo, and heptane and dodecanethiol were from Merck. Cadmium and manganese bis(ethyl-2-hexyl)sulfosuccinate [$Cd(AOT)_2$ and $Mn(AOT)_2$] were synthesized in our laboratory as described previously.[33]

Apparatus. Photoluminescence spectra were recorded with a Spex fluorolog (1681). An Oxford cryostat with a controller (ITC502) was used to control the sample temperature (77−300 K). Optical absorption spectra were obtained with a Cary (1E) and HP 8452A UV−visible spectrophotometer. Energy dispersive spectrometry (EDS) measurements were made with a Link AN 10,000. A JEOL (100 kV) Model JEM 100CX II was used for transmission electron microscopy (TEM) and electron diffraction. The mean diameter, D_m, and the standard deviation, σ_m, were derived from an average number of 500 particles.

* All correspondence to this author.
† Laboratoire SRSI, URA CNRS 1662.
‡ CEA-CE Saclay, DRECAM-SCM.
⊗ Abstract published in *Advance ACS Abstracts,* September 15, 1997.

S1089-5647(97)00978-4 CCC: $14.00

TABLE 1: Different Synthesis Modes: w, y, D_m, t_{dod}, and t_{ext} Are the Water Content, Composition, Average Particle Diameter, Size Distribution, Addition Time, and Extraction Time, Respectively

	synthesis mode								
	i				ii			iii	
w	5	10	20	40	40	40	40	10	10
y	various values of y				0	0.05	0.10	0.05	0.05
D_m (nm)	1.8	2.7	2.9	3.2	3.8	4	4.2	2.5	2.8
σ/D_m	0.16	0.16	0.15	0.1	0.13	0.11	0.12	0.15	0.16
t_{dod} (h)	0	0	0	0	0	0	0	0	1.5
t_{ext} (h)	0	0	0	0	48	48	48	0	1.5
name	I	II	III	IV	V	VI	VII	VIII	IX

III. Synthesis and Control Parameters.

Diluted magnetic semiconductors are synthesized using reverse micelles. Coprecipitation takes place on mixing two micellar solutions having the same water content, $w = [H_2O]/[AOT]$: 0.1 M Na(AOT) containing S^{2-} ions, and a mixed micellar solution containing $Cd(AOT)_2$, $Mn(AOT)_2$, and Na(AOT). An excess of sulfur ions is used in the syntheses ($x = ([Cd^{2+}] + [Mn^{2+}])/[S^{2-}] = 1/2$), at various ratios of $Mn(AOT)_2$ and $Cd(AOT)_2$.

To simplify the text, particles described in this paper are either indicated by the synthesis mode (described below in i, ii, and iii) or by a number when there are differences in the same synthesis mode. The details are given in Table 1.

After mixing the two micellar solutions, the procedure differs as follows.

(i) Dodecanethiol is immediately added to the micellar solution (designated $t_{dod} = 0$ in Table 1). This results, at the interface, in a selective surface reaction between the thio derivative and cadmium and manganese ions. The particles are extracted immediately from micelles (designated $t_{ext} = 0$ in Table 1), and the surfactant is removed by ethanol addition. The nanocrystallites coated by dodecanethiol are dispersed in a mixture of two solvents (isopentane−methylcyclohexane, 3v/v) forming an optically clear glass at low temperature. The average size of the coated particles increases with increasing water content in the medium in which the particles are synthesized (particles I, II, III, IV). Figure 1A shows histograms plots from TEM patterns. These clearly indicate an increase in the particle size with increasing water content. Syntheses at fixed water content and various $Mn(AOT)_2$ concentrations induce formation of $Cd_{1-y}Mn_yS$ with constant size over a range of compositions (Figure 1B).

(ii) Immediately after synthesis dodecanethiol is added ($t_{dod} = 0$) and the nanocrystallites remain in the micellar solution for 48 h. Then, the particles are extracted from micelles by using the same procedure as described above ($t_{ext} = 48$ h). This preparation method induces formation of particles with an average diameter of 4 nm, which is larger than that obtained by immediate extraction (particle IV).

(iii) Nanocrystallites are kept in the micellar solution for 90 min ($t_{dod} = 90$ mn), and then dodecanethiol is added and the particles are extracted ($t_{ext} = 90$ mn) as described above.

For all the samples prepared, the composition, y, is determined by energy dispersion spectroscopy, EDS. The nanocrystal structure is determined from electron diffraction. The nanoparticles are characterized by a zinc blende structure, whereas the bulk phase has a wurtzite structure. A similar change in the structure between the bulk phase and nanocrystals is observed for CdS.[34−36]

IV. Results

IV.1. Spectroscopic Measurements of Particles Extracted Immediately after Synthesis. IV.1.1. Variation of the Bandgap with Size and Composition. In the synthesis mode designated i, the size of the coated particles increases with increasing micellar water content in the synthesis medium. For a fixed composition, a red-shift in the absorption spectrum with increasing particle size is observed (Figure 1C). This is a direct result of the quantum confinement effects.[5−18] For a given average particle diameter, the absorption spectrum differs with composition, y, (Figure 1D).

From the absorption spectra shown in Figure 1, the direct bandgap of nanocrystallites is obtained by the following equation:[37]

$$\sigma h\nu = (h\nu - E_g)^{1/2} \quad (1)$$

where σ is the extinction coefficient and E_g is the bandgap energy. For a given composition, there is an increase in the bandgap energy with decreasing particle size, as shown in Figure 2. This is due to the quantum size effect.

For a given particle size, the bandgap does not vary monotonically with composition, as is observed for most semiconductor alloys:[38] It decreases and then increases (Figure 2). Similar behavior has been observed in the bulk phase[28] and films.[39] With nanocrystals, the minimum depth is more pronounced, and its depth increases with decreasing particle size (Figure 2).

In most II−VI diluted magnetic semiconductors, the minimum of the bandgap energy is observed.[27] It is attributed to exchange interactions of the conduction and valence band electrons with the Mn^{2+} d electrons.

For bulk $Zn_{1-y}Mn_ySe$, Bylsma et al.[30] related the energy bandgap to temperature and susceptibility by

$$E_g(y,T) = E_{g(0)} - AT^2/(T + B) + \Delta E y - b\chi(y)T \quad (2)$$

where $E_{g(0)}$, $\chi(y)$ and T are the band edge energy without Mn^{2+}, the susceptibility of the material, and temperature, respectively. ΔE is the variation of bandgap energy assuming a linear relationship between pure ZnSe and pure MnSe. A, B, and b are constants. A and B depend on the material, and b takes into account the exchange interactions between the Mn^{2+} d electrons and band electrons.

The bandgap energy variation with composition was determined for $Cd_{1-y}Mn_yS$ bulk[28] and film.[39] By using eq 2, the best fit between the experimental data and calculation is obtained for b values of 98 eV g Oe emu^{-1} K^{-1} and 85 eV g Oe emu^{-1} K^{-1}, respectively (Figure 2).

For nanocrystals, we assume that eq 2 is valid. The A and B values are determined from the variation of the bandgap energy with temperature and are independent of the material size (see below); to simulate eq 2, we use the theoretical bulk susceptibility, $\chi(y)$, as calculated by the equation given in ref 29. These values are not known for nanocrystals. The best fit with the experimental data is obtained for large b values. For 1.8 and 3.2 nm, it is 880 eV g Oe emu^{-1} K^{-1} and 330 eV g Oe emu^{-1} K^{-1}, respectively. These large values compared to those obtained in the bulk and in film (Table 2) indicate significant exchange interactions between the Mn^{2+} d electrons and the band electrons. The b value markedly increases with decreasing particle size. We attribute this to a quantum size effect.

IV.1.2. Variation of the Bandgap Energy with Temperature. The bandgap energy variation of bulk semiconductors with temperature was studied extensively.[40] This energy

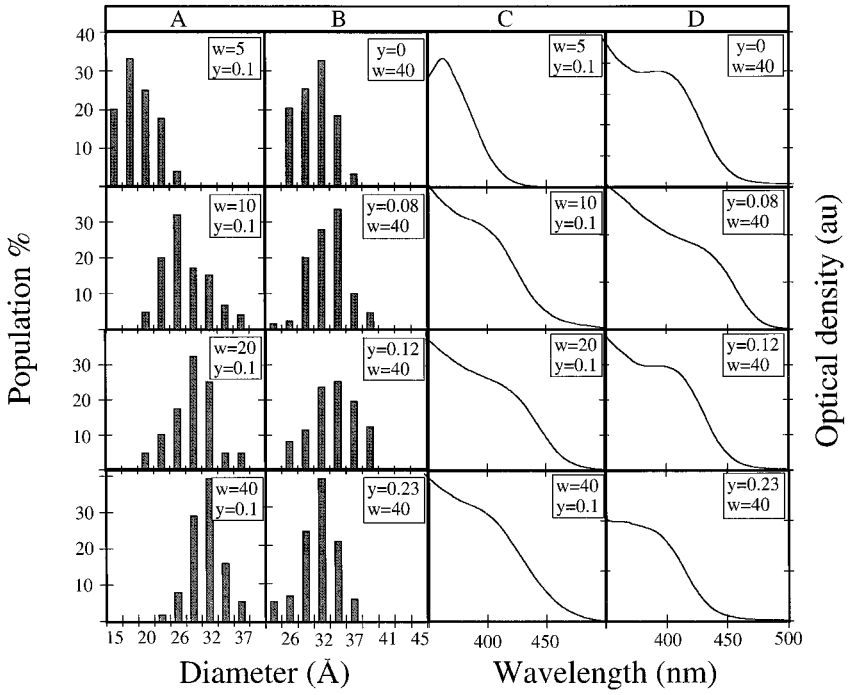

Figure 1. Size distribution and absorption spectra of $Cd_{1-y}Mn_yS$ particles synthesized at various water contents ($w = 0-40$) and various manganese concentrations ($y = 0-0.23$).

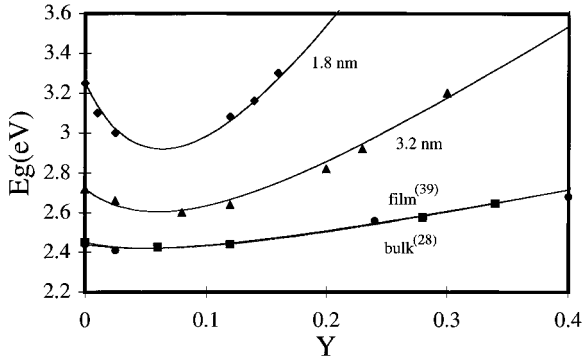

Figure 2. Variation of the bandgap energy with composition for various particles size, bulk,[28] and thin film.[39] The line is obtained from the best fit of experimental data to eq 2.

TABLE 2: Variation of the Parameter *b*, Derived from Simulation of Bandgap Evolution by Eq 2, with Particle Size

D_m	1.8	3.2	4	film[39]	bulk[28]
b (eV g Oe emu^{-1} K^{-1})	880	330	190	98	85

decreases with increasing temperature, and this is attributed to the relative position of the conduction and valence bands due to dilatation of the lattice with increasing temperature and to electron−lattice interactions. The bandgap energy is related to temperature by the following equation:[40]

$$E_g(T) = E_g(T=0) - AT^2/(T + B) \qquad (3)$$

where $E_g(T)$, $E_g(T = 0)$ are the bandgap energies at T and 0 K, respectively. A and B are constants related to the material (parameters A and B used in eqs 3 and 2 are the same). For bulk $Cd_{1-y}Mn_yS$, A is 5×10^{-4} ev K^{-1}.[28]

The $Cd_{1-y}Mn_yS$ nanocrystal absorption spectra in a range of sizes and compositions were recorded at various temperatures between 300 and 77 K. Figure 3 shows a shift to a lower bandgap energy with increasing temperature. The A and B values are derived from the best fit of eq 3 to the experimental data. They are close to those obtained for the bulk phase (Table 3).

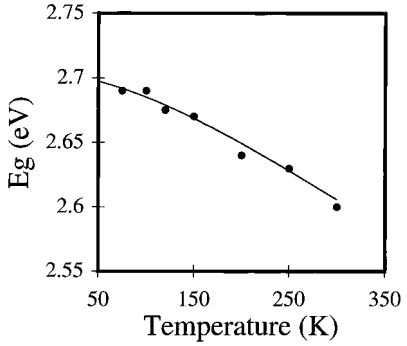

Figure 3. Variation of 3 nm $Cd_{0.92}Mn_{0.08}S$ nanoparticle bandgap energy with temperature.

TABLE 3: Variation with *y* Composition of (i) A and B Factors Obtained from the Best Fit of Experimental Data to Eq 3 and (ii) Bandgap Energy Determined from Absorption and PLE Spectra Recorded at 77 K

D_m (nm)	1.8	3.2	4	4	4	bulk[28]
y	0.05	0.05	0	0.05	0.1	0.1
A (eV K^{-1}) $\times$ 0.10^4	4.8	5.6	4.7[a]	5.2[a]	6.3	5
B (K)	250	220	200[a]	240[a]	270	
E_g(77K)$_{abs}$ (eV)	3.2	2.7			2.75	2.55
E_g(77K)$_{PLE(Mn^{2+})}$ (eV)				2.62	2.65	
E_g(77K)$_{PLE(trap)}$ (eV)	2.9	2.7	2.68	2.67	2.7	

[a] Determined from variation of excitation spectra with temperature.

IV.1.3. Variation of $Cd_{0.95}Mn_{0.05}S$ Nanosized Particle Luminescence with Size. The photoluminescence (PL) spectra of $Cd_{0.95}Mn_{0.05}S$ nanocrystals in the range of sizes from 1.8 nm (particles I) to 3.2 nm (particles IV) recorded at 77 K are shown in Figure 4.

For 1.8 nm particles, the PL spectrum has a large band centered at 600 nm. This luminescence is similar to that obtained without Mn^{2+} ions included in a CdS matrix and is attributed to CdS defect states.[9,18,5,41,42] The photoluminescence excitation (PLE) spectrum of trap emission shows a well resolved excitonic peak (Figure 4). A slight shift in the PLE

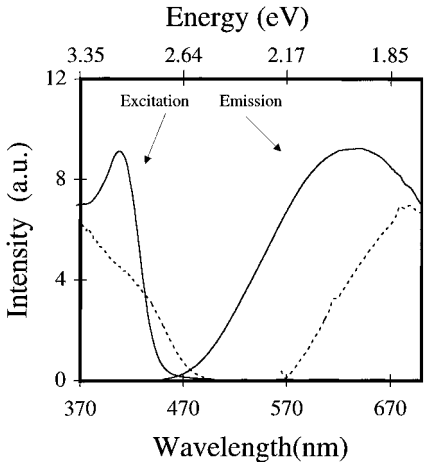

Figure 4. PL (λ_{ex} = 400 nm) and PLE (λ_{em} = 600 nm) spectra, recorded at 77 K, of $Cd_{0.95}Mn_{0.05}S$ nanoparticles with different sizes: 1.8 nm (—) and 3.2 nm (···).

spectra with the emission wavelength is obtained. This is due to the size distribution.

Similar behavior is observed for 3.2 nm crystallites with good correlation between the bandgap energy determined from absorption and PLE spectra (Table 3). As expected from Dannhauser et al.,[43] the CdS trap emission is red-shifted when the particle size increases.

The bandgap energies are derived from the PLE spectra and compared to those obtained from absorption spectra at the same temperature (77 K). Table 3 shows quite a good agreement between these two techniques.

The PL spectra are fitted by assuming two Gaussian curves as described before.[49] From this, the half-width of Mn^{2+} luminescence is 0.23 eV. This value is in good agreement with those determined for Mn^{2+} luminescence in the bulk phase[44] and in $Zn_{1-y}Mn_yS$ nanoclusters.[19−24]

Hence, with nanosized particles synthesized by using mode i (particles I, II, III, IV) there is emission from CdS traps and no luminescence due to the presence of isolated Mn^{2+} in CdS matrixes.

IV.2. Spectroscopic Measurements of Particles Extracted 48 h after Syntheses. In this section we present data obtained with nanocrystals synthesized by the second procedure (type ii). The average particle size is 4 nm, and composition varies from $y = 0$ to 0.14.

IV.2.1. Luminescence Data at Various Temperatures at a Given Composition, $y = 0.05$. The PL spectrum of $Cd_{0.95}Mn_{0.05}S$ nanocrystals (particles VI) was recorded at various temperatures. At room-temperature, emissions due to CdS defect states are observed (Figure 5). As expected, the decrease in temperature induces an increase in the PL intensity. However, a new luminescence band with a peak centered at 580 nm appears, as is clearly shown in Figure 5. This is attributed to Mn^{2+} emission in a tetrahedral coordination (transition $^4T_1$ to $^6A_1$).[29,44]

At a given temperature (77 K), the PLE spectra recorded at 580 and 700 nm are similar to the nanoparticles VI absorption spectrum. A small shift toward the larger wavelengths can be seen when the excitation spectrum is recorded at 580 nm compared to that observed at 700 nm (Figure 6). This is attributed to a slight increase in the size distribution when the particles are synthesized by mode ii.

IV.2.2. Effect of Composition on the Spectroscopic Data, at a Given Particle Size. The absorption spectrum of $Cd_{1-y}Mn_yS$ crystallites (V, VI, VII) was recorded at various temperatures for different compositions. As expected, the

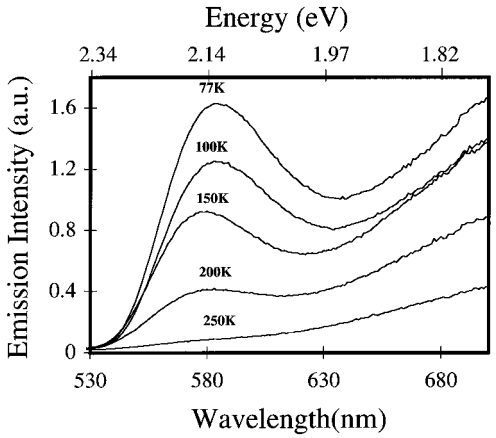

Figure 5. Variation of 4 nm $Cd_{0.95}Mn_{0.05}S$ nanoparticle PL spectra with temperature.

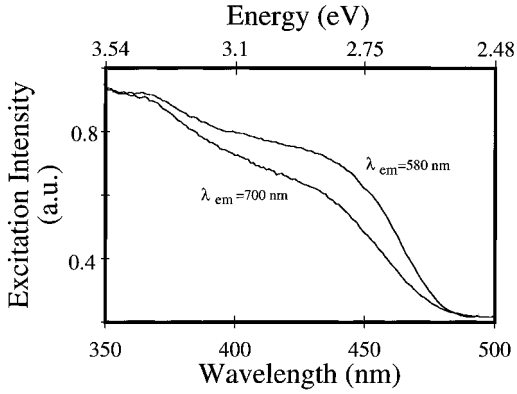

Figure 6. PLE spectra of 4 nm $Cd_{0.95}Mn_{0.05}S$ nanoparticles, recorded at 77 K at λ_{em} = 580 nm and λ_{em} = 700 nm.

bandgap energy increases with decreasing temperature. *A* and *B* values are derived by fitting eq 3 (Table 3). They are similar to those obtained for smaller sizes and to the bulk phase.

PL and PLE spectra were recorded at 77 K. Without Mn^{2+} included in CdS matrixes (particles V), there are two luminescence peaks at 465 and 700 nm, as shown in Figure 7A. The weak emission band at shorter wavelengths is attributed to the direct transition from the conduction to the valence band.[45−47] This indicates that the particle crystallinity is rather high. The main luminescence band is broad and is attributed to CdS trap emission.

When Mn^{2+} ions are included in a CdS matrix (particles VI) the direct transition disappears and a new fluorescence band centered at 580 nm (Figure 7B,C) is seen.

The increase in the 580 nm PL intensity with increasing composition is followed by a decrease for compositions above 0.1. The plot of the relative ratio of 580 nm to 700 nm PL intensities with composition (contribution of the emission due to CdS at $y = 0$ is extracted) shows the appearance of a maximum at $y = 0.1$ (Figure 8A). This is related to the number of isolated (without any manganese−manganese interactions) Mn^{2+}. The number of these Mn^{2+}, y_{eff}, with composition y has been calculated by Kreitman et al.[48] (Figure 8B). The y_{eff} variation with composition has a maximum around 0.1. However, the shape of the relative intensity variation with composition (Figure 8A) differs from that for y_{eff} (Figure 8B).

Figure 7 shows a shift of the PLE spectrum to longer and then to shorter wavelengths with increasing Mn^{2+} content. Such behavior is similar to that observed by absorption spectroscopy with the appearance of a minimum in the bandgap energy for $y = 0.05-0.1$. The bandgap energies, determined from PLE

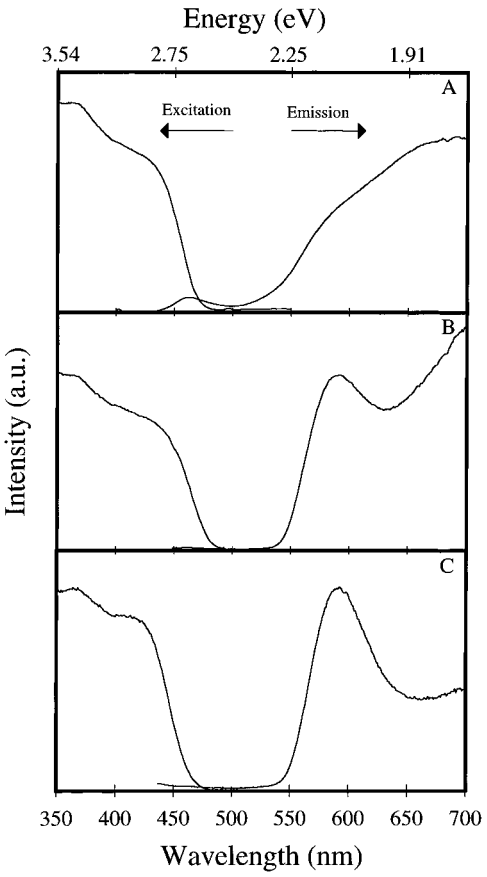

Figure 7. PL (λ_{ex} = 400 nm) and PLE (λ_{em} = 580 nm) spectra, recorded at 77 K at various compositions: $y = 0$ (A), 0.05 (B) and 0.1 (C). The average particle diameter is 4 nm.

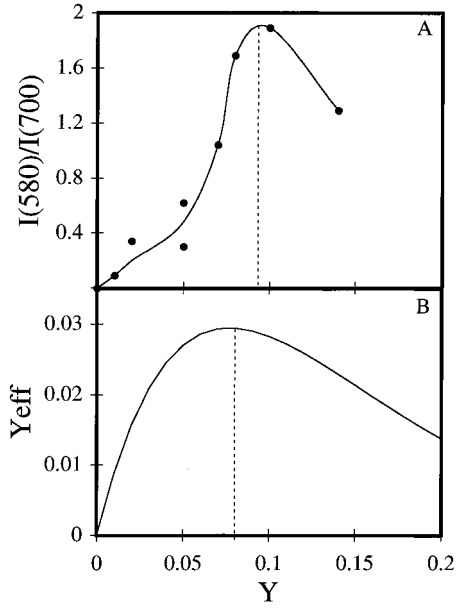

Figure 8. Variation of 4 nm $Cd_{1-y}Mn_yS$ nanoparticle relative emission intensity I_{580}/I_{700} (A) and y_{eff} (B) with composition, y.

spectra (by using eq 1), agree with those measured at the same temperature (77 K) from the absorption spectra (Table 3) and pass through a minimum with increasing y.

For CdS quantum dots[49] the PL intensity dependence on temperature obeys an Arrhenius equation as

$$I_{77K}/I(T) = A'T^{-0.5}\exp(-E_a/KT) \qquad (4)$$

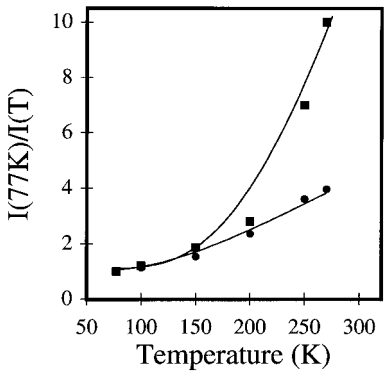

Figure 9. Variation of the PL relative intensity obtained at 77 K and T (K), ($I(T = 77\text{ K})/I(T)$), with temperature. The intensities are observed at 580 nm (■) and 700 nm (●), respectively. The line indicates the best fit between the experimental data and eq 4.

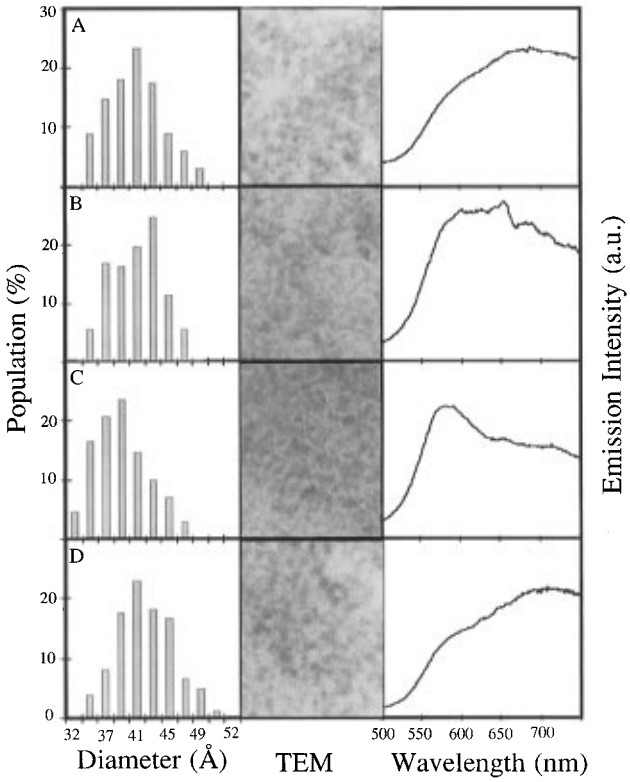

Figure 10. Histogram, TEM, and PL spectrum of $Cd_{0.95}Mn_{0.05}S$ nanocrystallites after annealing in the range 30−120 °C. After 2 h annealing at 30 °C (A), 60 °C (B), 80 °C (C), and 120 °C (D).

where I_{77K} and I are the relative PL intensities of fluorescence recorded at 77 K and at T (K), respectively.

For $Cd_{1-y}Mn_yS$ we assume, as observed with CdS quantum dots, that (i) eq 4 is valid for alloy semiconductor quantum dots; (ii) the $Cd_{1-y}Mn_yS$ luminescence does not markedly change below 77 K.

The activation energy, E_a, is obtained from the best fit of eq 4 to the experimental data for 580 and 700 nm emission wavelengths (Figure 9). At $y = 0$, the same activation energies are obtained at 580 and 700 nm, whereas the values differ in the presence of Mn^{2+} (Table 4). This confirms the emission from two distinct centers.

IV.2.3. Annealing Effect on the Luminescence Spectra. $Cd_{0.95}Mn_{0.05}S$ nanocrystal powder with 4 nm average size (particles VI) was annealed for 2 h in the temperature range from 30 to 120 °C. After annealing, the size and composition were determined by TEM and EDS, respectively. The histograms plotted from TEM patterns indicate no changes in the

TABLE 4: Variation of Activation Energy Determined from the Change of Luminescence at 580 and 700 nm with Temperature. The Average Particle Diameter Is 4 nm and *y* Varies from 0 to 0.1

	y		
	0	0.05	0.10
$E_{a(580\ nm)}$ (meV)	32	60	62
$E_{a(700\ nm)}$ (meV)	32	32	32

average size. In the annealing range from 30 to 120 °C, the particle size remains unchanged. The composition, y, does not vary in the annealing range from 30 to 80 °C, whereas at 120 °C most Mn^{2+} ions are released from the CdS matrix.

After annealing it is rather difficult to disperse the nanocrystals in a solvent. This prevents the formation of an optically clear solution. The fluorescence spectra of nanocrystal powder were thus recorded, at room temperature, by reflectivity measurements.

At 30 °C, emission centered at 700 nm due to CdS defect states is observed (Figure 10A). By progressively increasing the annealing temperature, the PL spectra change with a progressive appearance of luminescence centered at 580 nm (Figure 10B,C). A 580 nm maximum intensity is reached at 80 °C. In these cases, *y* remains constant (Table 5). This appearance of Mn^{2+} luminescence is attributed to an increase in the disorder inside the CdS matrix with a migration of Mn^{2+} to the surface. At 120 °C, 580 nm emission disappears and only trap emissions remain, as shown in Figure 10D.

IV.3. Influence of the Aging Time on the Fluorescence Spectra. From the data described above, it seems obvious that the aging plays an important role in the appearance of the Mn^{2+} luminescence. To demonstrate this, nanocrystals were synthesized by using a third procedure (iii). Addition of dodecanethiol and the extraction process are carried out either immediately after synthesis (particles VIII) or after 90 min (particles IX). The nanocrystals are dispersed in a solvent.

At room temperature, the PL of particles VIII is characterized by a weak and broad spectrum with a maximum centered at 650 nm (Figure 11). It is attributed to CdS trap emissions of nanoparticles with 2.5 nm average size. The particles IX (aged) are characterized by a broader PL spectrum, with a maximum centered at 680 nm and the appearance of a shoulder around 580 nm (arrow in Figure 11). The comparison of histograms of particles VIII (inset, Figure 11: $t_{ex} = 0$ h) and IX (inset, Figure 11: $t_{ex} = 1.5$ h) shows a slight increase in the particle size after aging. Hence, the red-shift of the PL spectrum of particles IX compared to VIII is due to the CdS trap emissions for larger particles. The shoulder is attributed to the emission of isolated Mn^{2+} in the CdS matrix. To confirm the appearance of luminescence due to Mn^{2+} when the particles are aged, the PL spectra were recorded at 77 K. The particles VIII PL spectrum remains the same as that obtained for pure CdS particles with the same size and is attributed to emission from defect states. Conversely, the PL spectrum of particles IX is blue-shifted with a marked increase in intensity. The Mn^{2+} luminescence bandwidth is obtained from fitting two Gaussians (Mn^{2+} and trap emission) and is 0.23 eV. This confirms the appearance of luminescence due to Mn^{2+} when the particles are aged. However, the PL band due to emission of defect states remains rather broad. This is attributed to a low nanoparticle crystallinity and to the increase in the surface defects. That CdS trap emission remains large at low temperature indicates that only a part of the emissions due to defects participates in the energy transfer from CdS to Mn^{2+} ions.

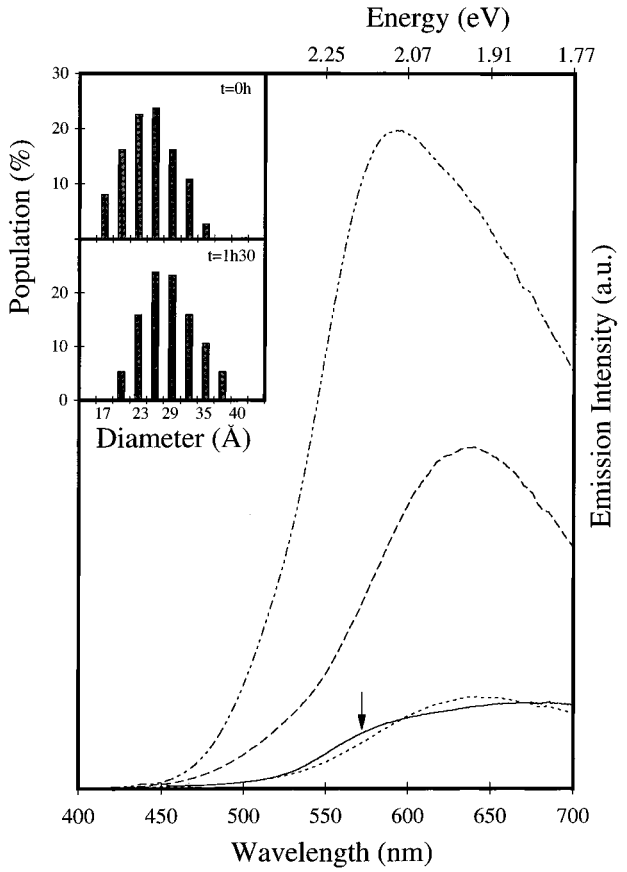

Figure 11. Histograms and PL spectra recorded at 300 and 77 K for $Cd_{0.95}Mn_{0.05}S$ nanoparticles extracted at $t_{ext} = 0$ ($T = 300$ K (- - -), $T = 77$ K (— — —) and $t_{ext} = 1.5$ h ($T = 300$ K (—), $T = 77$ K (— - -).

TABLE 5: Variation of Composition (*y*), Diameter (D_m), and Size Distribution with Annealing Temperature

	T_a(°C)			
	30°	60°	80°	120°
y	0.05	0.06	0.05	not detected
D_m(nm)	4.1	4	3.8	4.2
σ/D_m	0.13	0.09	0.12	0.13

V. Discussion

The bandgap energy decreases with increasing composition, *y*, and reaches a minimum. This has been observed in the bulk phase and is attributed to the interactions between the Mn^{2+} d electrons and the valence and conduction band electrons. The minimum composition, y_{min}, slightly shifts toward the higher *y* values with decreasing particle size. The y_{min} values vary from 0.055 to 0.075. However the depth of the minimum is more pronounced with decreasing particle size (Figure 2). This is attributed to an increase in the electronic interactions at smaller particle sizes. Assuming eq 2 is valid for nanocrystals, the term *b* represents these interactions. The *b* value decreases with increasing particle size and does not reach those determined for the bulk phase or film (Table 2). From this, it is concluded that the electronic interactions between manganese and the conduction and valence bands markedly increase with decreasing particle size.

In the bulk phase, traces of Mn^{2+} included in DMS material induce luminescence of isolated Mn^{2+} arranged in a tetrahedral coordination. This is attributed to energy transfer from CdS to Mn^{2+} ions.

Dodecanethiol-coated nanocrystals extracted from reverse micelles immediately after synthesis and dispersed in a solvent (synthesis mode i)show a broad PL emission. This is observed

for various compositions, particle sizes, and excitation wavelengths. The luminescence is attributed to CdS trap emissions and is red-shifted when the particle size increases (Figure 4). Particles I and IV do not show luminescence due to isolated Mn^{2+}. Only luminescence due to the CdS defect states is observed. This result is rather surprising, and no obvious explanations can be given. This could be related to the strong interactions between the Mn^{2+} d electrons and the band electrons. This is strongly supported by the high values of *b* factors (Table 2) obtained from the variation of bandgap energy with size and composition (Figure 2). This cannot be attributed to the formation of a mixture of CdS and MnS nanoparticles. In the latter case, the change in the bandgap energy with increasing composition would never show a minimum, as observed in Figure 2.

When the coated particles are aged in the micellar solution (synthesis mode ii), the behavior differs as observed above: In the presence of Mn^{2+} ions in the CdS matrix, the CdS trap luminescence is observed at room temperature. On decreasing the temperature a new luminescence band centered at 580 nm appears (Figure 5). The relative intensity of the peak at 580 nm compared to trap emissions increases with increasing *y* and reaches a maximum at $y = 0.1$ (Figure 8). The activation energies derived at 580 nm and for CdS trap emissions differ (Table 4). The half width of the PL band centered at 580 nm obtained from fitting two Gaussians is similar to that obtained in the bulk phase. These data confirm the appearance of a new fluorescence band. It is well-known that CdS emission due to defect states is red-shifted when the particle size increases.[43] Comparison of $Cd_{1-y}Mn_yS$ PL spectra observed under various experimental conditions (Figures 7 and 11) shows a red-shift in the CdS trap emission with an increase in the particle size, whereas the Mn^{2+} luminescence position remains fixed and independent of the particle size.

The $Cd_{1-y}Mn_yS$ PL spectra responsible for Mn^{2+} and CdS trap emissions provide a technique for assessing the size distribution and their relative contributions to total luminescence efficiency in a given size nanocrystal sample. The following data confirm that the energy transfer occurs from s−p electron hole pair band states to the Mn^{2+} d states: (i) The ratio of Mn^{2+} to CdS trap intensities increases with increasing composition, *y*. (ii) The bandgap energies measured by PLE spectra using Mn^{2+} and CdS traps emission as probes are in good agreement with those determined from absorption spectroscopy. (iii) For a given particle size, the bandgap energies, determined from excitation spectra, vary with composition, as observed from absorption spectra, with a minimum around $y = 0.05-0.10$.

If we compare the PL data obtained with coated particles extracted immediately (syntheses i) and those aged (syntheses ii) in reverse micelles, it is clear that the luminescence due to isolated Mn^{2+} is observed when the particles are aged or annealed.

By annealing particles in the temperature range from 30 to 80 °C, the particles VII retain their manganese content (Table 5) and their sizes (Figure 11). However a marked change in the PL spectra is observed. With particles annealed at 30 °C, CdS emissions, due to defect states, are observed at room temperature. On increasing annealing temperatures from 60 to 80 °C, there is a progressive appearance of Mn^{2+} fluorescence, as shown in Figure 11. This is observed at room temperature, whereas without annealing, the Mn^{2+} fluorescence is observed at low temperature (Figures 5 and 7). As there is no change in the particle size and composition, the appearance of Mn^{2+} luminescence at room temperature is attributed to a progressive phase transition inside the CdS matrix: Before annealing the Mn^{2+} ions are well dispersed inside the CdS matrix, whereas afterward Mn^{2+} ions move progressively to the nanocrystal surface, which would favor the Mn^{2+} emission. It must be noted that Mn^{2+} stays in the tetrahedral coordination. This displacement is confirmed by the fact that no Mn^{2+} ions are detectable by EDS when the particles are annealed at 120 °C and CdS trap emissions are observed.

For particles annealed at 120 °C, it is reasonable to assume that Mn^{2+} traces remain inside the matrix. However, fluorescence due to isolated Mn^{2+} is not observed. This confirms that specific preparation conditions are needed to obtain Mn^{2+} luminescence in nanocrystals. From these data, we conclude that the average location of Mn^{2+} changes markedly with the preparation mode and controls the appearance of Mn^{2+} luminescence.

From the comparison of the luminescence data obtained for particles with different synthesis modes, we can make the following remarks.

(i) The appearance of Mn^{2+} emission is obtained when the particles are aged. The aging mode plays an important role. Several processes have to be taken into account. When particles are not protected by thiododecane (synthesis iii), the growth of the particles is fast and the crystallinity rather low. Immediately after synthesis with mode (i), the particle size is 3.2 nm (particles IV), whereas after 48 h in micellar solution (particles V−VII) it varies from 3.8 to 4.2 nm. This indicates that the growth process is slow. It permits preparation of particles with a higher crystallinity. This explains the appearance of a direct transition at 77 K (Figure 7A). In this case, the particles are coated with dodecanethiol and the nanocrystal surface is protected by a selective reaction between the thio derivatives and cadmium ions. This limits the growth of particles. However, the S−Cd bond is not as strong as a covalent bond. There is an exchange of thio derivatives between the surface and solvent.[50,51] This is more pronounced when an excess of thio derivatives is present in the bulk solvent (as is the case in our experimental conditions). The growth of the nanocrystals takes place during the exchange.

(ii) The appearance of Mn^{2+} emission does not depend on the particle size in the range between 1.8 and 4 nm. As a matter of fact, particles I and IV do not emit at 580 nm, whereas IX does.

(iii) The Mn^{2+} PLE spectrum ($\lambda_{em} = 580$ nm) of particles VII is red-shifted compared to that due to defect states (700 nm). This indicates that the Mn^{2+} emission is more efficient for larger particles.

The increase in intensity of the peak centered at 580 nm with increasing composition can be attributed to an increase, at low *y* values, of the number of isolated Mn^{2+} ions. The maximum is reached at $y = 0.08$. This corresponds to the maximum number of isolated Mn^{2+}. However the shape of the curve (Figure 7A) differs from the calculated amount of free Mn^{2+}- (Figure 7B). This could be explained by the fact that y_{eff} is calculated for a perfect bulk crystal with a random distribution of Mn^{2+} in the CdS matrix. In the nanosize range, about 50% of the atoms are at the interface, which induces defect creation. Furthermore the crystallinity of nanoparticles is less than that of the bulk crystal.

Similar Mn^{2+} luminescence has been observed with $Zn_{1-y}Mn_yS$ nanocrystals[19−24] and $Cd_{1-y}Mn_ySe$ nanocrystallites.[25,26] In all the published experimental conditions, the Mn^{2+} fluorescence is observed when the particles are aged and/or have been subjected to a thermal treatment: (i) Wang et al.[19] synthesized $Zn_{1-y}Mn_yS$ nanocrystals inside a glass matrix with a thermal treatment.

(ii) Bhargava et al.[20−22] synthesized $Zn_{1-y}Mn_yS$ nanoparticles from coprecipitation of their salt derivatives. To prevent growth and to disperse the nanocrystals, either PMMA {poly(methyl methacrylate)}or methacrylic acid was added. An increase in the Mn^{2+} fluorescence was observed under UV irradiation for several hours. The authors attributed this enhancement in Mn^{2+} photoluminescence to passivation of the surface. From our data, this could be explained as particle aging. (iii) Sooklal et al.[23] prepared $Zn_{1-y}Mn_yS$ by a coprecipitation reaction. To obtain 5 nm nanoclusters from which Mn^{2+} fluorescence is observed, the particle were aged for 5 h. Since no protecting agent was added to the aqueous solution, the particle stability is lower and the number of defects at the interface is probably high.

Taking into account these published data[19−23] and those presented in this paper, we deduce that Mn^{2+} luminescence takes place when the particles are aged. The Mn^{2+} luminescence does not seem to be a result of the high degree of localization that occurs in these confined structures. It can be attributed to surface passivation or to displacement of Mn^{2+} from the inside to the surface of the particles. This could be related to the marked increase in the Mn interactions when the particle size decreases.

VI. Conclusion

We have presented absorption and photoluminescence spectra for particles from 2 to 4 nm in size and *y* composition from 0 to 0.3, respectively. When particles are extracted from reverse micelles immediately after coating, the variation of the bandgap energy with composition markedly differs with the particle size. It is attributed to a large increase in the interactions between the Mn^{2+} d electrons and the valence and conduction band electrons. The bandgap variation with temperature follows the same behavior as the bulk phase. When the $Cd_{1-y}Mn_yS$ is immediately extracted from reverse micelles, the luminescence is characterized by the CdS shallow trap which is due to defects of the states. If they are kept in the solution for 48 h, the average particle diameter slightly increases from 3 to 4 nm. The variation of the bandgap energy with composition follows the same behavior as presented for smaller particles with fewer sp−d electron interactions. At low temperatures, Mn^{2+} photoluminescence is then observed. It increases with composition to reach a maximum at $y = 0.1$, which corresponds to the maximum isolated ions inside the CdS matrix. The activation energy is higher (62 meV) than that due to the trap emissions (32 meV). Annealing these particles, in the temperature range 30−80 °C, does not induce changes in size and composition. The Mn^{2+} photoluminescence is observed at room temperature. Similar behavior is observed when the particles are aged.

Acknowledgment. The authors would to thank Dr. P. Lavallard for fruitful discussions.

References and Notes

(1) Special issue of *Chemistry of Materials*, **1996**, 8.
(2) Pileni, M. P. *J. Phys. Chem*. **1993**, *97*, 6961.
(3) Lisiecki, I.; Pileni, M. P. *J. Am. Chem. Soc*. **1993**, *115*, 3887.
(4) Petit, C.; Lixon, P.; Pileni, M. P. *J. Phys. Chem*. **1993**, *97*, 12974.
(5) Motte, L.; Petit, C.; Lixon, P.; Boulanger, L.; Pileni, M. P. *Langmuir* **1992**, *8*, 1049.
(6) Brus, L. E. *J. Chem. Phys*. **1983**, *79*, 5566.
(7) Rossetti, R; Ellison, J. L.; Bigson, J. M.; Brus, L. E. *J. Chem. Phys*. **1984**, *80*, 4464.
(8) Nozik, A. J.; Williams, F.; Nenadocic, M. T.; Rajh, T.; Micic, O. I. *J. Phys. Chem*. **1985**, *89*, 397.
(9) Petit, C.; Pileni M. P. *J. Phys. Chem*. **1988**, *92*, 2282
(10) Kayanuma, Y. *Phys. Rev. B* **1988**, *38*, 9797.
(11) Lippens, P. E.; Lannoo M. *Phys. Rev. B* **1989**, *39*, 10935.
(12) Petit, C.; Lixon, P.; Pileni M. P. *J. Phys. Chem*. **1990**, *94*, 1598.
(13) Hu, Y. Z.; Lindberg, M.; Koch, S. W. *Phys. Rev. B* **1990**, *42*, 1713.
(14) Wang, Y.; Herron, N. *Phys. Rev. B* **1990**, *41*, 6079.
(15) Bawendi, M. G.; Steigerwald, M. L.; Brus, L. E. *Annu. Rev. Phys. Chem*., **1990**, *41*, 477.
(16) Rama Krishna, M. V.; Friesner, R. A. *J. Chem. Phys*. **1991**, *95*, 8309.
(17) Nosaka, J. *J. Phys. Chem*. **1991**, *95*, 5054.
(18) Pileni, M. P.; Motte, L.; Petit, C. *Chem. Mater*. **1992**, *4*, 338.
(19) Wang, Y.; Herron, N.; Moller, K.; Bein, T. *Solid State Commun*. **1991**, *77*, 33.
(20) Bhargava, R. N.; Gallagher, D.; Welker, T. *J. Lumin*. **1994**, *60*, *61*, 275.
(21) Bhargava, R. N.; Gallagher, D.; Hong, X.; Nurmikko, A. *Phys. Rev. Lett*. **1994**, *72*, 416.
(22) Bhargava, R. N. *J. Lumin*. **1996**, *70*, 85.
(23) Sooklal, K.; Cullum, B. S.; Angel, S. M.; Murphy, C. J. *J. Phys. Chem*. **1996**, *100*, 4551.
(24) Khosravi, A. A.; Kundu, M.; Kuruvilla, B. A.; Shekhawat, G. S.; Gupta, R. P.; Sharma, A. K.; Vyas, P. D.; Kulkarni, S. K. *Appl. Phys. Lett*. **1995**, *67*, 2506.
(25) Yanata, K.; Susuki, K.; Oka, Y. *Jpn. J. Appl. Phys*. **1993**, *32*, Suppl. 32−3, 384.
(26) Oka, Y; Yanata, K. *J. Lumin*. **1996**, *70*, 35.
(27) Furdyna, J. K.; Kossut, J. *Semiconductors and semimetals*; Academic Press: New York, 1988; Vol. 25.
(28) Ikeda, M.; Itoh, K.; Hisano, S. *J. Phys. Soc. Jpn*. **1968**, *25*, 455.
(29) Furdyna, J. K. *J. Appl. Phys*. **1988**, *64*, R29.
(30) Bylsma, R. B.; Becker, W. M.; Kossut, J.; Debska, U. *Phys. Rev. B* **1986**, *33*, 8207.
(31) Larson, B. E.; Hass, K. C.; Ehrenreich, H.; Carlsson, A. E. *Solid State Commun*. **1985**, *56*, 347.
(32) Levy, L.; Hochepied, J. F.; Pileni, M. P. *J. Phys. Chem*. **1996**, *100*, 18332.
(33) Petit, C.; Lixon, P.; Pileni, M. P. *Langmiur* **1991**, *7*, 2620.
(34) Cizeron, J.; Pileni, M. P. *J. Phys. Chem*. **1995**, *99*, 17410.
(35) Gandais, M. Private communication, 1994.
(36) Vogel, W.; Urban, J.; Kundu, M.; Kulkarni, S. K. *Langmuir* **1997**, *13*, 827.
(37) Wang, Y.; Herron, N. *J. Phys. Chem*. **1991**, *95*, 525.
(38) Muhamad, M. R. *Jpn. J. Appl. Phys*. **1993**, *32*, 3385.
(39) Tsai, C. T.; Chen, S. H.; Chuu, D. S.; Chou, W. C. *Phys. Rev. B* **1996**, *54*, 11555.
(40) Varshni, Y. P. *Physica* **1967**, *34*, 149.
(41) Kotov, N. A.; Meldrum, F. C.; Wu, C.; Fendler, J. H. *J. Phys. Chem*. **1994**, *98*, 2735.
(42) Coffer, J. L.; Bigham, S. R.; Pinizzotto, R. F.; Yang, H. *Nanotechnology* **1992**, *3*, 69.
(43) Dannhauser, T. O'Neil, M.; Johansson, K.; Whitten, D.; McLendon, G. *J. Phys. Chem*. **1986**, *90*, 6074.
(44) Gumlich, H.-E. *J. Lumin*. **1981**, *23*, 73.
(45) Katsikas, L.; Eychmüller, A.; Weller, H. *Chem. Phys. Lett*. **1990**, *172*, 201.
(46) Grätzel, M.; Ramsden, J. J. *J. Chem. Soc., Faraday Trans*. **1984**, *80*, 919.
(47) Tian, Y.; Wu, C.; Fendler, J. H. *J. Phys. Chem*. **1994**, *98*, 4913.
(48) Kreitman, M. M.; Barnett, D. L. *J. Chem. Phys*. **1965**, *43*, 364.
(49) Wang, Y.; Herron, N. *J. Phys. Chem*. **1988**, *92*, 4988.
(50) Jennings, G. K.; Laibinis P. E. *Langmuir* **1996**, *12*, 6173.
(51) Laibinis, P. E.; Fox, M. A.; Folkers, J. P.; Whitesides, G. M. *Langmuir* **1991**, *7*, 3167.